Article

Cell

Species-Independent Attraction to Biofilms through Electrical Signaling

Graphical Abstract

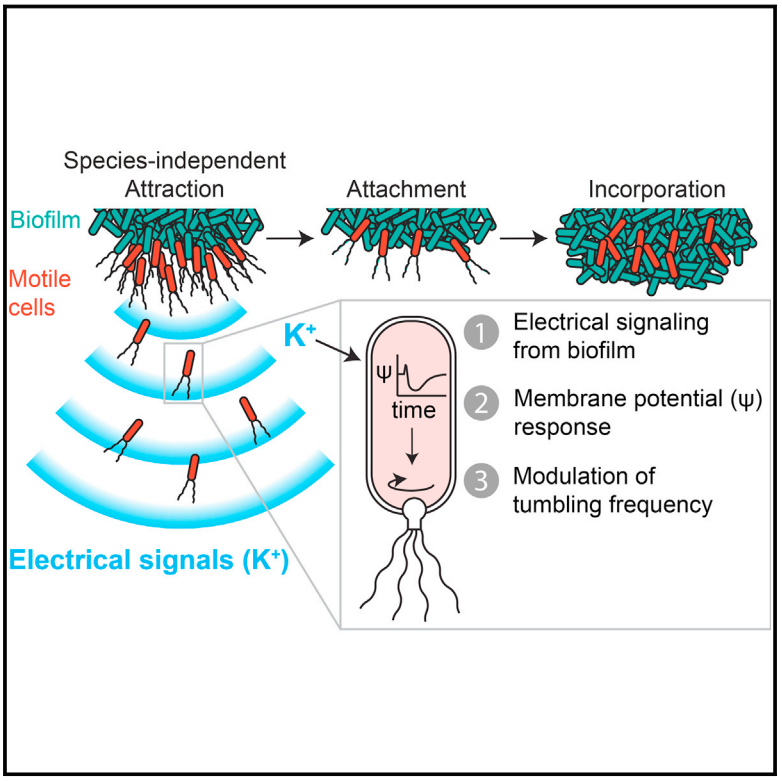

Highlights

- Electrical signaling within biofilms attracts distant motile cells
- Attraction is caused by membrane-potential-dependent modulation of tumbling frequency
- Electrical signaling is generic, resulting in species-independent attraction
- Attraction leads to incorporation of diverse species into a pre-existing biofilm

Authors

Jacqueline Humphries, Liyang Xiong, Jintao Liu, ..., Heidi A. Arjes, Lev Tsimring, Gürol M. Süel

Correspondence

gsuel@ucsd.edu

In Brief

Ion-channel-based electrical signaling by *B. subtilis* biofilms attracts distant motile cells, leading to incorporation of diverse species into a pre-existing biofilm community.

Humphries et al., 2017, Cell *168*, 200–209
January 12, 2017
http://dx.doi.org/10.1016/j.cell.2016.12.014

CellPress

Cell

Article

Species-Independent Attraction to Biofilms through Electrical Signaling

Jacqueline Humphries,[1] Liyang Xiong,[2] Jintao Liu,[1] Arthur Prindle,[1] Fang Yuan,[1] Heidi A. Arjes,[3,4] Lev Tsimring,[5,6] and Gürol M. Süel[1,5,6,7,8,*]

[1]Division of Biological Sciences, University of California, San Diego, La Jolla, CA 92093, USA
[2]Department of Physics, University of California, San Diego, La Jolla, CA 92093, USA
[3]Department of Bioengineering, Stanford University, Stanford, CA 94305, USA
[4]Department of Microbiology and Immunology, Stanford University School of Medicine, Stanford, CA 94305-5101, USA
[5]BioCircuits Institute, University of California, San Diego, La Jolla, CA 92093, USA
[6]San Diego Center for Systems Biology, University of California, San Diego, La Jolla, CA 92093, USA
[7]Center for Microbiome Innovation, Jacobs School of Engineering, University of California, San Diego, La Jolla, CA 92093, USA
[8]Lead Contact
*Correspondence: gsuel@ucsd.edu
http://dx.doi.org/10.1016/j.cell.2016.12.014

SUMMARY

Bacteria residing within biofilm communities can coordinate their behavior through cell-to-cell signaling. However, it remains unclear if these signals can also influence the behavior of distant cells that are not part of the community. Using a microfluidic approach, we find that potassium ion channel-mediated electrical signaling generated by a *Bacillus subtilis* biofilm can attract distant cells. Integration of experiments and mathematical modeling indicates that extracellular potassium emitted from the biofilm alters the membrane potential of distant cells, thereby directing their motility. This electrically mediated attraction appears to be a generic mechanism that enables cross-species interactions, as *Pseudomonas aeruginosa* cells also become attracted to the electrical signal released by the *B. subtilis* biofilm. Cells within a biofilm community can thus not only coordinate their own behavior but also influence the behavior of diverse bacteria at a distance through long-range electrical signaling.

INTRODUCTION

Bacteria within biofilms can coordinate their behavior through distinct forms of communication (Shapiro 1998; Waters and Bassler, 2005; Brameyer et al., 2015; Liu et al., 2015). The best characterized cell-to-cell signaling process in bacteria is known as quorum sensing (Miller and Bassler, 2001). Recently, another cell-to-cell communication mechanism based on ion channel-mediated electrical signaling has also been described (Prindle et al., 2015). This electrical signaling has been shown to facilitate communication within a biofilm community (Liu et al., 2015; Prindle et al., 2015). Specifically, cells within *B. subtilis* biofilms can actively relay extracellular potassium signals, producing electrical waves that propagate through the biofilm and coordinate metabolic states, thereby increasing collective fitness (Prindle et al., 2015; Liu et al., 2015). These findings provoke the question of whether such extracellular signals could extend beyond the biofilm, resulting in long-range interactions that could affect distant bacteria that are not part of the biofilm. Here, we utilized a microfluidic approach to investigate whether electrical signals generated within the biofilm can influence the behavior of other bacteria that share the same aqueous environment. In particular, we hypothesized that electrical signals could direct bacterial motility through altering the membrane potential. Such long-range signaling could provide a generic mechanism for bacterial communities to exert control over the motile behavior of distant cells.

RESULTS

Periodic Attraction of Distant Motile Cells to Electrically Oscillating Biofilms

We began by measuring the interaction dynamics between a biofilm and motile cells in a large microfluidic chamber (3 mm × 3 mm × 6 μm) (Figure S1). Specifically, we grew a biofilm in the microfluidic chamber until it reached the size (over one million cells) at which oscillations emerge (Liu et al., 2015). We then introduced motile cells into the chamber and noticed that they were periodically attracted to the electrically oscillating biofilm (Movie S1). To accurately discriminate between biofilm and motile cells, we then introduced fluorescently labeled motile cells (constitutively expressing a fluorescent protein) into the growth chamber, again after biofilm formation (Figure 1A). To determine the relationship between motile cell attraction and electrical oscillations in the biofilm (Prindle et al., 2015), we quantified the membrane potential of biofilm cells by using the previously characterized fluorescent cationic dye Thioflavin T (ThT) (Figure 1A) (Prindle et al., 2015). This charged reporter dye diffuses across the membrane according to the membrane potential and thereby acts as a Nernstian voltage indicator of bacterial membrane potential (Plásek and Sigler, 1996). This approach revealed that the periodic increase in motile cell density at the biofilm edge accurately tracks the oscillations in biofilm membrane potential

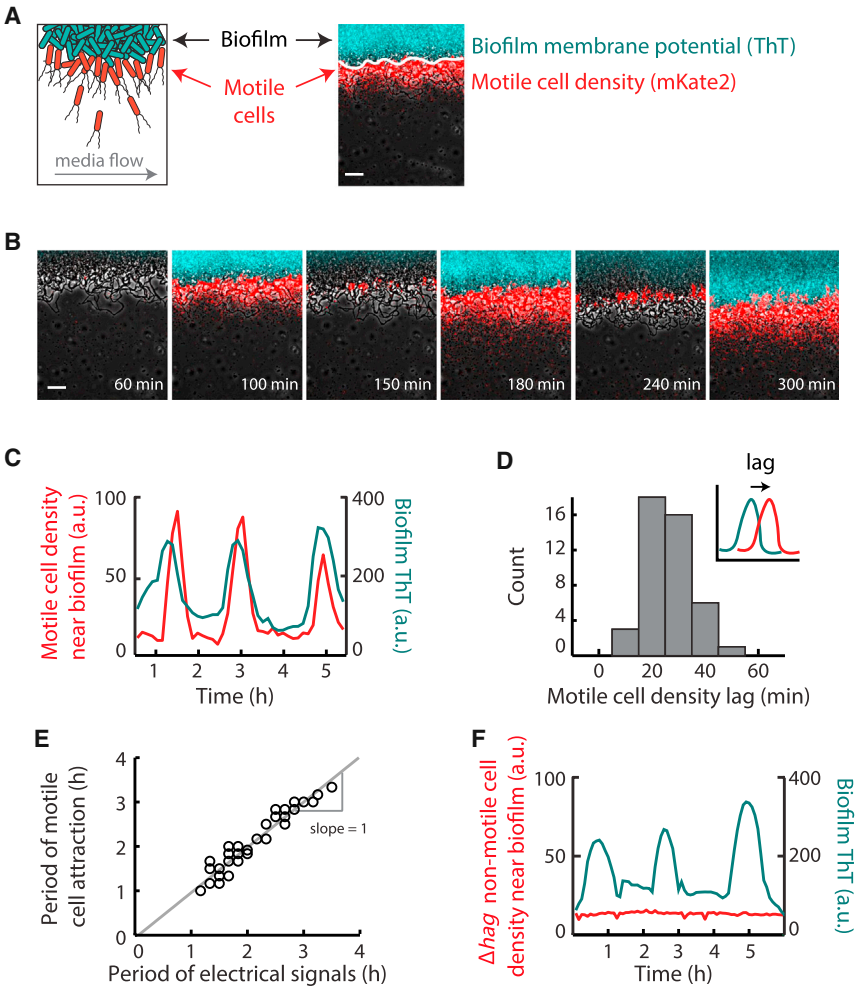

Figure 1. Distant Motile Cells Are Periodically Attracted to an Electrically Oscillating Biofilm

(A) Illustration of motile cell interaction with a biofilm within a shared microfluidic growth chamber (see Figure S1). Media flows in the direction indicated by the gray arrow, at a rate of 12 μm/s. Membrane potential changes are reported by Thioflavin T (ThT, pseudocolored cyan), a cationic dye that acts as a Nernstian voltage indicator (Prindle et al., 2015). ThT fluorescence increases when the cell becomes more inside-negative, making ThT fluorescence inversely related to the membrane potential. Motile cells (pseudocolored red) express a fluorescent protein mKate2 from the $P_{hyperspank}$ promoter induced with 1 mM IPTG. Motile cell density is measured using mKate2 fluorescence (only present in motile cells) in the 100 μm region outward from the biofilm edge (indicated as a solid white line, see Quantification and Statistical Analysis in the STAR Methods). Scale bar, 50 μm.

(B) Filmstrip showing the edge of a biofilm that is located on the top of each image. Images depict periodic motile cell attraction to an electrically oscillating biofilm and subsequent passive dispersal away from the biofilm. Gray (phase contrast), cyan (membrane potential), red (motile cells). Scale bar, 50 μm.

(C) Time series of motile cell density (red) near the biofilm edge together with membrane potential reporter ThT measured within the biofilm (cyan). Time series shows that motile cell density changes periodically along with electrical oscillations within the biofilm. Time series is representative of three independently reproduced experiments.

(D) Histogram of the time between peaks in biofilm electrical activity and peaks in motile cell attraction (motile cell density lag). Motile cell peaks occur on average 26.4 ± 8.8 min after the initiation of electrical oscillations within the biofilm (mean ± SD, n = 44 pulses, see Quantification and Statistical Analysis in the STAR Methods). Inset: illustration of the quantification method for motile cell density lag. Motile cell density lag is defined as the time between the electrical pulse (cyan) and the motile cell pulse (red), represented with an arrow (see Quantification and Statistical Analysis in the STAR Methods).

(E) Scatter plot of the periods of electrical oscillations within biofilms (peak to peak) and the periods of co-occurring pulses in motile cell attraction (peak to peak). Periods of motile cell attraction correlate with natural variations in the periods of electrical oscillations within biofilms (see Quantification and Statistical Analysis in the STAR Methods, Pearson correlation coefficient = 0.96, n = 33 periods).

(F) Time series of non-motile (Δ*hag*, red) cell density together with biofilm membrane potential (cyan). Time series shows no periodic attraction of non-motile cells to an oscillating biofilm. Time series is representative of three independently reproduced experiments.

See also Figure S2 and Movies S1 and S2.

(Figures 1B and 1C; Movie S2). In particular, the peak accumulation of motile cells at the biofilm edge slightly lags the peak of electrical signaling in the biofilm by 26 ± 9 min (mean ± SD, n = 44 pulses; Figures 1C and 1D). Furthermore, the period of motile cell attraction to the biofilm edge tracks with the natural variation in the period of electrical signaling within biofilms (Figure 1E). We observed no attraction of motile cells to biofilms that had not yet initiated electrical oscillations (Figure S2), suggesting that electrical signaling plays a critical role in motile cell attraction. In addition, functional motility machinery in distant cells is also required, as non-motile cells lacking the flagellin gene *hag* showed no attraction to electrically oscillating biofilms (Figure 1F). Together, these results show that electrical oscillations generated by the biofilm are correlated in time with periodic attraction of distant motile cells to the biofilm.

Sufficiency of Extracellular Potassium in Directing Cell Motility

We next asked whether the observed attraction of motile cells was due to changes in extracellular potassium generated during biofilm oscillations (Prindle et al., 2015). Utilizing the microfluidic device, we directly tested whether potassium signals were sufficient to influence motile cells. Specifically, we investigated whether we could redirect motile cells away from the biofilm by providing an alternative and stronger source of extracellular potassium. Accordingly, we transiently flowed media

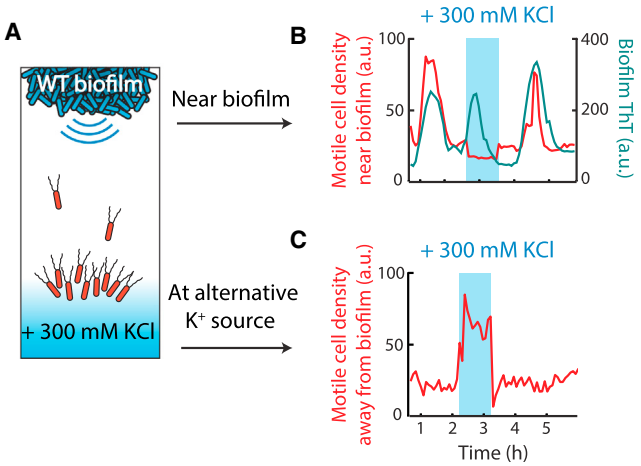

Figure 2. Extracellular Potassium Is Sufficient to Direct Motility

(A) An alternative potassium source is introduced into the growth chamber (blue shading) to redirect motile cells away from an oscillating biofilm (see the STAR Methods). Arrows indicate the two regions where cell density was evaluated for the time series shown in (B) and (C).

(B and C) Time series showing redirection of motile cells (in red) away from the electrically oscillating biofilm (shown in B, cyan) and toward the alternative potassium source (MSgg + 300 mM KCl, shown in C) that was introduced at a distance from the biofilm edge. The alternative potassium source (indicated by blue shading) was generated for 1 hr during the peak of electrical activity in the biofilm when motile cell attraction is typically maximal. Time series shown are representative of eight independently reproduced experiments.

supplemented with potassium into the region most distant from the biofilm (Figure 2A). This alternative potassium source was introduced during a peak in biofilm electrical activity (maximal motile cell attraction) (Figure 2B). We find that instead of being attracted to the biofilm, motile cells now accumulated at the competing potassium source (Figures 2B and 2C). Removal of this alternative potassium source restored motile cell attraction to the biofilm in the subsequent pulse of electrical activity (Figure 2B). These results demonstrate that changes in extracellular potassium gradients are sufficient to direct motile cell behavior.

We then began to investigate the potential mechanism by which waves of extracellular potassium released by the biofilm could influence the motility of distant cells. It is known that changes in extracellular potassium lead to changes in the cell's membrane potential and proton motive force (Bakker and Mangerich, 1981; Booth, 1985; Abee et al., 1988). The proton motive force in turn influences bacterial motility by controlling the frequency of tumbling events that enable a biased random walk along a concentration gradient (Berg and Brown, 1972; De Jong et al., 1976; Manson et al., 1977; Miller and Koshland, 1980). The relationship between extracellular potassium, membrane potential, and tumbling frequency of motile cells suggests a possible mechanism for the observed attraction of motile cells to biofilms.

The Role of the Potassium Ion Channel in Motile Cell Attraction

To determine the mechanism of motile cell attraction, we first confirmed that potassium ion channel activity in the biofilm generates the extracellular potassium signal that results in motile cell attraction. Complete deletion of the potassium ion channel YugO interferes with *B. subtilis* biofilm formation (Lundberg et al., 2013; Prindle et al., 2015). Therefore, we turned to a previously characterized mutant strain (Δ*trkA*), which only lacks the TrkA gating domain of the YugO potassium ion channel and exhibits diminished electrical signaling (Prindle et al., 2015) (Figure 3B). We find that biofilms formed by this mutant strain have a 75% ± 4% (mean ± SD, n = 3 experiments for each genotype) lower electrical signaling amplitude when compared to wild-type biofilms (Figures 3A and 3B). Correspondingly, motile cell attraction to *ΔtrkA* biofilms is reduced by 70% ± 9% (mean ± SD, n = 3 experiments for each genotype) (Figure 3D). Therefore, we find a direct correlation between the weaker electrical signal generated by *ΔtrkA* biofilms and the corresponding decrease in motile cell attraction. These results show that potassium ion channels in biofilm cells play an important role in generating the electrical signal that attracts motile cells.

Motile Cell Membrane Potential Influences Attraction to Biofilms

We speculated that attraction of motile cells depends not only on the signal emitted by the biofilm, but also the sensitivity of motile cells to the potassium signal. Specifically, the sensitivity to changes in extracellular potassium depends on the resting membrane potential of the cell (Hille, 2001).We anticipated that motile cells with a more negative resting membrane potential would be more sensitive to the potassium signals emitted by the biofilm. Accordingly, we deleted the major *B. subtilis* potassium pump (KtrA) in motile cells. Potassium pumps are responsible for maintaining the high intracellular concentration of potassium ions and thus play a key role in establishing the resting membrane potential (Castañeda-García et al., 2011; Gries et al., 2013). Consequently, *ΔktrA* motile cells would have a reduced ability to pump in positively charged potassium ions and thus have a relatively more negative membrane potential. Indeed, we find a 57% ± 6% (mean ± SD, n = 2 experiments) more negative membrane potential in the *ΔktrA* strain relative to wild-type (Figure S3). When exposed to wild-type biofilms with nearly identical electrical oscillation amplitudes, we observed more than 2-fold (239% ± 25%, mean ± SD, n = 8 experiments) increase in attraction of *ΔktrA* motile cells, compared to wild-type motile cells (Figures 3A, 3C, and 3D). These results show that attraction also depends on the membrane potential-mediated sensitivity of motile cells to the potassium signals generated by the biofilm.

Membrane Potential and Tumbling Frequency of Distant Cells Depend on Biofilm Oscillations

Next, we established that electrical activity within the biofilm can alter the membrane potential of distant cells. We confirmed that an electrically active biofilm generates a dynamic potassium gradient, as reported by the potassium-specific fluorescent dye Asante Potassium Green 4 (APG-4) (Figures 4A and S4). We then utilized distant cells that by chance adhered to the microfluidic chamber to measure membrane potential in individual cells over time without having to track their movement (Figure 4B). This allowed us to precisely measure the membrane potential dynamics of distant cells during an entire period of

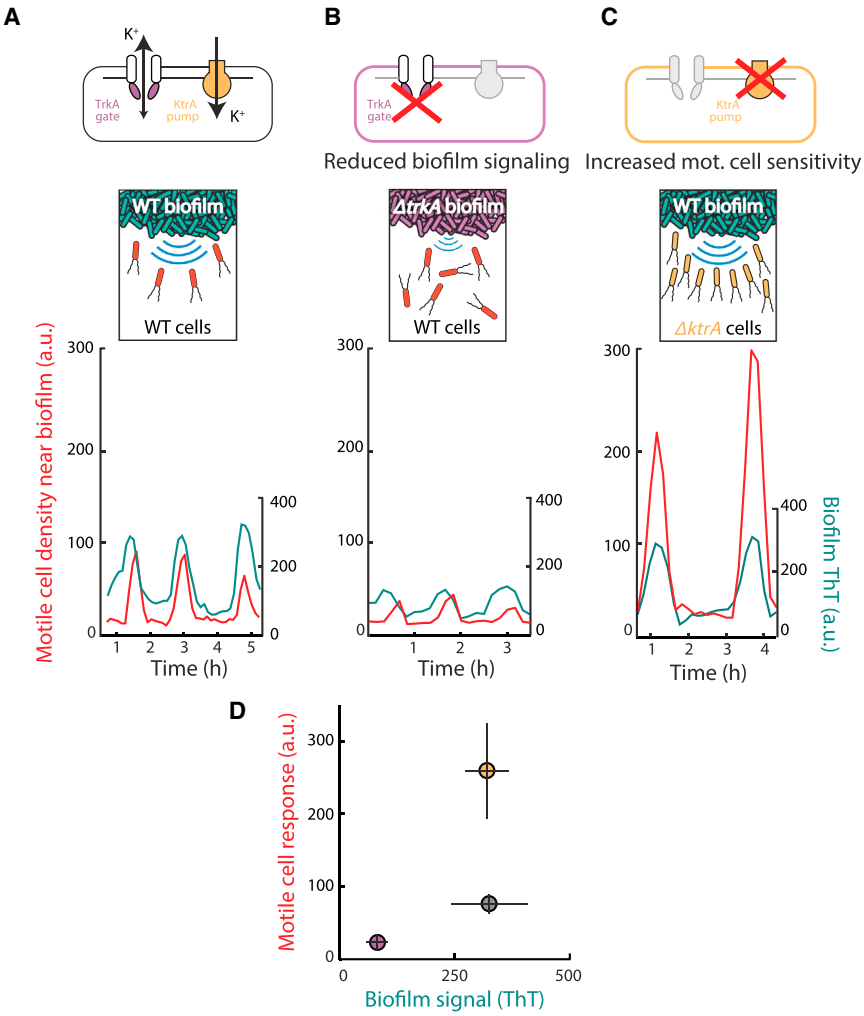

Figure 3. Motile Cell Attraction Depends Both on the Strength of Biofilm Electrical Signals and the Sensitivity of Motile Cells to These Signals

(A) Top: wild-type cells contain a potassium ion channel YugO that is gated by a TrkA domain, and a potassium ion pump KtrA. Bottom: wild-type (WT) motile cell attraction (in red) to electrical oscillations from a WT biofilm (in cyan, same data as Figure 1, shown here for comparison to B and C).

(B) Top: the TrkA gating domain of YugO was deleted in biofilm cells, resulting in reduced biofilm signaling. Bottom: time series of WT motile cell response to Δ*trkA* biofilm electrical oscillations shows reduced oscillation amplitude ($n = 6$, $p = 2.20 \times 10^{-7}$, two sample t test), and reduced motile cell attraction compared to a WT biofilm ($n = 3$, $p = 2.24 \times 10^{-7}$, two sample t test). Time series is representative of six independently reproduced experiments.

(C) Top: the potassium pump KtrA was deleted in motile cells, which leads to hyperpolarization (see Figure S3) and increased sensitivity to potassium signals. Bottom: time series of Δ*ktrA* motile cell response to WT biofilm electrical oscillations shows increased attraction ($n = 8$, $p = 6.66 \times 10^{-6}$, two sample t test) compared to WT motile cells responding to a WT biofilm (see A). WT biofilms in this experiment had similar oscillation amplitude as in (A) ($n = 3$, $p = 0.906$, two sample t test). Time series is representative of eight independently reproduced experiments.

(D) Plot of average peak biofilm signal versus average peak motile cell response for WT (gray circle) compared to Δ*trkA* (purple circle) and Δ*ktrA* (yellow circle) mutants shows that reducing the amplitude of the potassium signal reduces attraction, while increasing the sensitivity to the potassium signal increases attraction (mean ± SD, WT $n = 3$, Δ*trkA* $n = 6$, Δ*ktrA* $n = 8$, see Quantification and Statistical Analysis in the STAR Methods).

electrical signaling in the biofilm. We find that the membrane potential of these stationary cells becomes more negative during the peak of electrical oscillations in the biofilm (Figures 4C and 4D). Together, these data indicate that potassium waves generated by the biofilm can induce changes in the membrane potential of distant cells.

We then asked whether the tumbling frequency of individual motile cells also depends on the electrical activity of the biofilm. Using phase contrast imaging every 10 ms, we compared a total of 2,668 motile cell trajectories obtained specifically during a peak or trough of electrical oscillations in the biofilm (Figure 4E; Movie S3). This approach allowed us to determine the relationship between tumbling frequency of motile cells and the electrical signaling generated by the biofilm. During the peak of electrical activity in the biofilm, we observed that the tumbling frequency of motile cells was inversely related to their distance from the biofilm (Figure 4F). In other words, distant motile cells exhibited directional swimming, while cells already near the electrically active biofilm edge tumbled and thus remained at the biofilm edge. In contrast, there was no such spatial organization of tumbling frequencies during the trough in biofilm electrical activity (Figure 4F). These results suggest that the tumbling frequency of motile cells is altered by the spatio-temporal extracellular potassium gradient generated by the biofilm.

Agent-Based Mathematical Modeling Confirms that Extracellular Potassium Can Direct Motility

To integrate the above described multiple lines of experimental evidence into a coherent phenomenological framework, we turned to mathematical modeling. We utilized an electrophysiological model based on the mathematical framework developed by Hodgkin and Huxley (1952) to predict changes in membrane potential in response to extracellular potassium (Prindle et al., 2015) (see the STAR Methods for details). This model was constrained by our measurement of membrane potential dynamics observed in distant stationary cells (Figure 4D). We integrated this electrophysiological model with an agent-based physical model (Mather et al., 2010; Volfson et al., 2008) to simulate the motility of individual cells (see Figure 5 and STAR Methods for details of the agent-based model). In brief, cells were modeled as soft spherocylinders that moved according to Newton's law under the forces and torques caused by their own motility and

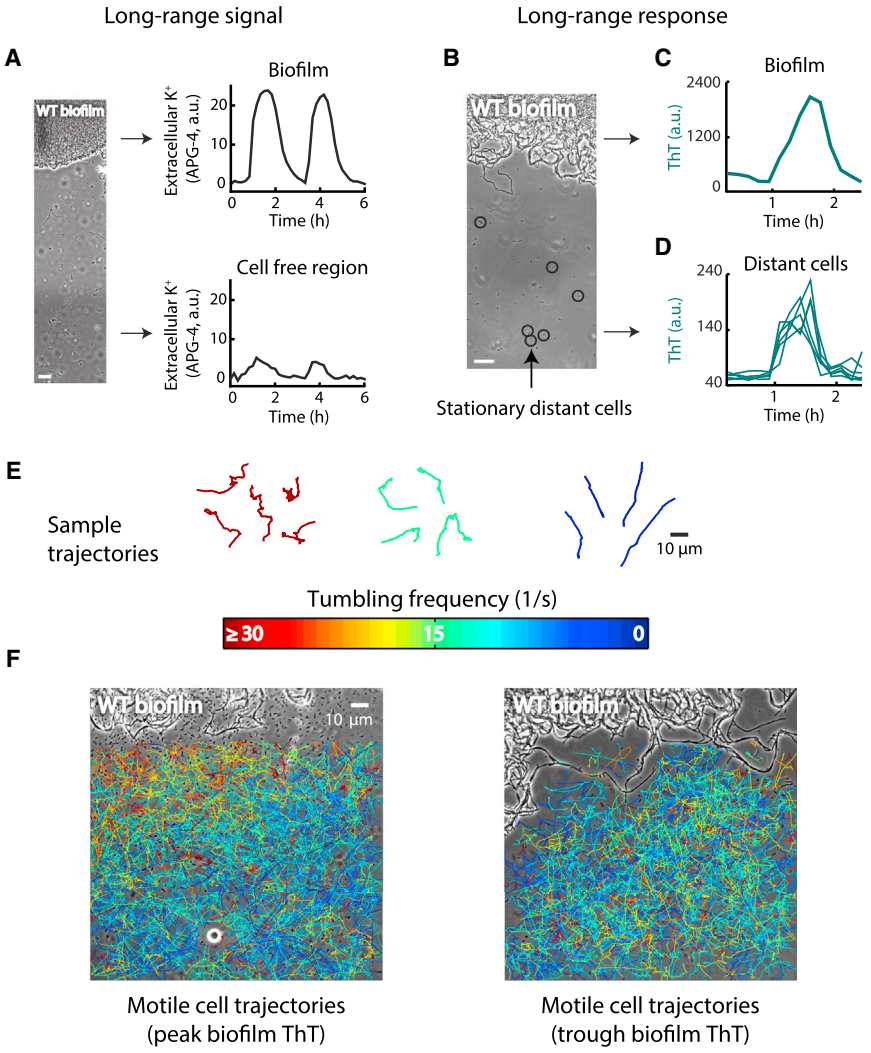

Figure 4. Extracellular Potassium Is a Long Range Signal that Can Influence the Membrane Potential and Tumbling Frequency of Motile Cells

(A) The fluorescent chemical dye Asante Potassium Green (APG-4) was used to track the extracellular concentration of potassium between cells in the biofilm and the surrounding cell free region. APG-4 fluorescence was measured over time at the regions shown in the phase image on the left. On the right, time series of APG-4 fluorescence intensity oscillations between cells in the biofilm (top), and in the cell-free region distant from the biofilm (bottom). Scale bar, 50 μm. See also Figure S4.

(B) Phase contrast image of a biofilm and distant stationary cells. The membrane potential of cells circled in black was tracked over time to determine the response to long-range signals emitted from the biofilm. Scale bar, 12 μm.

(C) Time series of a membrane potential (ThT) pulse in the biofilm.

(D) Time series of the co-occurring membrane potential pulse in distant cells shows membrane potential changes that are in phase with biofilm electrical oscillations.

(E) Individual motile cells were tracked over time and their motion was compiled into trajectories that trace their movement. To track motile cells, we used high frequency (10-ms interval) phase contrast imaging. Sample trajectories are shown for three different average tumbling frequencies and are colored based on their average tumbling frequency (1/s), according to the color scale shown below.

(F) Individual motile cells were tracked near the biofilm at both the peak and trough of electrical activity (n = 2,668 trajectories). Trajectories are colored based on their average tumbling frequency, and overlaid on a phase contrast image of the biofilm, the color scale is the same as in (E). Left: during a peak in electrical activity in the biofilm, motile cell tumbling frequencies are inversely related to distance from the biofilm, consistent with a biased random walk up a potassium concentration gradient. Right: during a trough in biofilm electrical activity, there is no relationship between motile cell tumbling frequency and distance from the biofilm. The biofilm is at the top of each image, scale bar applies to both images. Overlaid trajectories include cells that were tracked for at least 500 ms.

See also Table S1 and Movie S3.

contacts with other cells. In a departure from earlier models (Prindle et al., 2015; Mather et al., 2010; Volfson et al., 2008), each cell was endowed with a set of ordinary differential equations coupling its electrophysiological state with its motility (Figure 5A; STAR Methods). Using this model, we computed how a change in extracellular potassium altered the cell's membrane potential and how this in turn affected the tumbling probability of each motile cell (Figures 5A and S5) (De Jong et al., 1976; Manson et al., 1977; Miller and Koshland, 1980). Furthermore, the simulations contained non-motile biofilm cells that were assumed to alternate between acting as a source or sink of potassium (peak and trough electrical activity respectively) (Figure 5B, cyan and black cells, respectively). The spread of extracellular potassium through the medium was described by the standard diffusion equation (see the STAR Methods for details). Consistent with experimental results, simulations showed periodic attraction of distant motile cells to an electrically oscillating biofilm (Figure 5B; Movie S4). These modeling results demonstrate that an oscillating source (biofilm) of extracellular potassium can periodically attract motile cells by changing their membrane potential.

Our model was predominantly informed by measurements in stationary cells, providing the opportunity to independently validate modeling predictions through additional motile cell measurements. In particular, we tested the modeling prediction that motile cells moving along a spatial potassium gradient are expected to have a similar membrane potential profile as stationary cells responding to temporal changes of potassium (Figure 5C). In other words, motile cells during peak biofilm electrical activity should on average have a more negative membrane potential. To test this prediction, we measured the distribution of membrane potential in motile cells specifically at the attraction (peak) and non-attraction (trough) phases of the electrical oscillations in the biofilm. As predicted by our model, we find

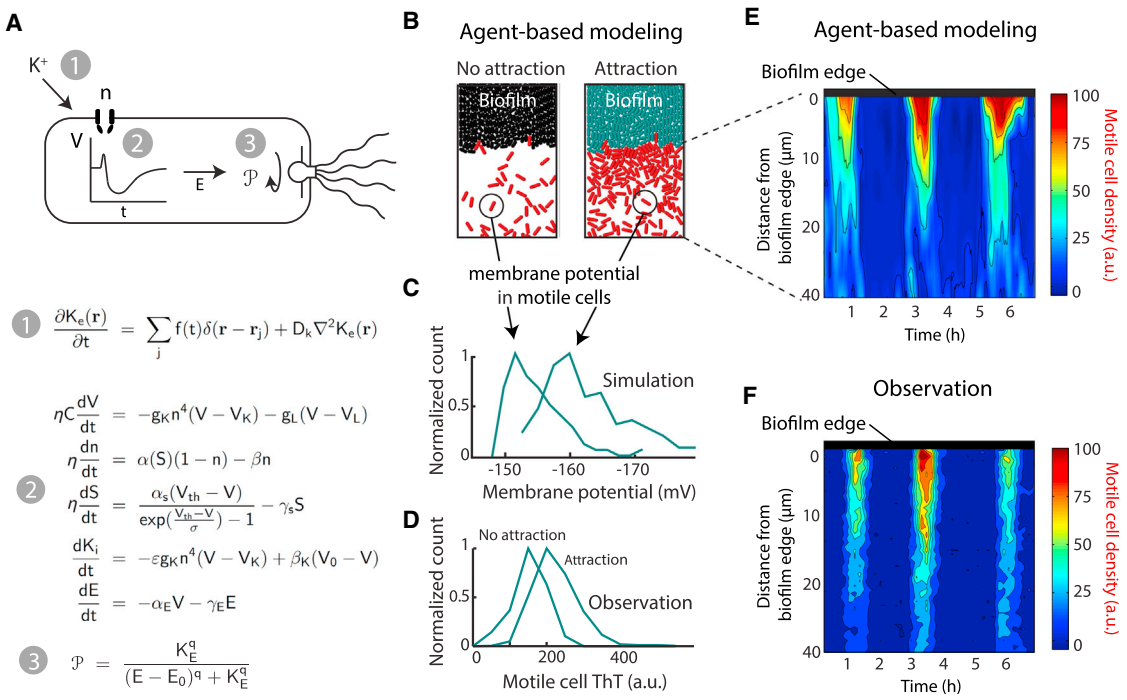

$$1\quad \frac{\partial K_e(\mathbf{r})}{\partial t} = \sum_j f(t)\delta(\mathbf{r}-\mathbf{r}_j) + D_k\nabla^2 K_e(\mathbf{r})$$

$$2\quad \begin{aligned} \eta C\frac{dV}{dt} &= -g_K n^4(V-V_K) - g_L(V-V_L)\\ \eta\frac{dn}{dt} &= \alpha(S)(1-n) - \beta n\\ \eta\frac{dS}{dt} &= \frac{\alpha_s(V_{th}-V)}{\exp(\frac{V_{th}-V}{\sigma})-1} - \gamma_s S\\ \frac{dK_i}{dt} &= -\varepsilon g_K n^4(V-V_K) + \beta_K(V_0-V)\\ \frac{dE}{dt} &= -\alpha_E V - \gamma_E E \end{aligned}$$

$$3\quad \mathcal{P} = \frac{K_E^q}{(E-E_0)^q + K_E^q}$$

Figure 5. Agent-Based Modeling of Motile Cell Attraction Driven by Electrical Signaling from Biofilms

(A) Top: schematic illustrating how extracellular potassium alters motility by changing the membrane potential. Step 1: extracellular potassium depolarizes the cell. Step 2: depolarization prompts adaptation by the cell leading to hyperpolarization. Step 3: hyperpolarization increases the proton motive force, thus directing motility by altering the tumbling frequency of the cell. Bottom: the computational model encompassing: (1) spatiotemporal reaction-diffusion model for the extracellular potassium K_e dynamics; (2) intracellular electrophysiological model for the cell membrane potential V, ion channel state n, metabolic stress S, intracellular potassium K_i, and energy needed to drive the flagellar motor E; and (3) discrete biomechanical model for individual cell motion influenced by their internal motility and interaction with other cells. The motility of individual cells is affected by the internal cellular state E via the change of the probability of tumbling $\mathcal{P}$. The details of the model and the model parameters can be found in the STAR Methods and Table S1. See also Figure S5.

(B) Two snapshots of the combined agent-based simulation show increased density of motile (red) cells near the biofilm during the peak of the attraction phase to the biofilm. Biofilm cells are colored according to their membrane potential during each time point, where cyan coloring indicates more negative membrane potential relative to black coloring.

(C) Distributions of membrane potential in motile cells from the computational model indicate that motile cell membrane potential is more negative during the peak of the attraction phase to the biofilm.

(D) Experimental data confirm the modeling prediction that the distribution of motile cell membrane potential (ThT, a.u.) is more negative during attraction to the biofilm compared to the non-attraction phase (see Quantification and Statistical Analysis in the STAR Methods).

(E) Plot of motile cell density in the first 40 μm away from the biofilm edge over time, obtained from agent-based modeling simulations of motile cell attraction. The region closest to the biofilm edge is located at the top of the plots for both (E) and (F) and distance from the biofilm edge increases moving downward.

(F) Experimental data show similar motile cell density dynamics in the first 40 μm away from the biofilm edge.

See also Movie S4.

that motile cells have on average a more negative membrane potential in the attraction phase (Figure 5D). These data show that similar to stationary cells, the membrane potential of motile cells also depends on the electrical activity of the biofilm. In addition, we find that the motile cell density profile as a function of time and distance from the biofilm is consistent with modeling predictions (Figures 5E and 5F). Together, these results further validate the mathematical model and allow us to establish a coherent framework to interpret experimental observations.

Electrically Mediated Attraction Applies across Distinct Bacterial Species

The membrane potential plays a general role in bacterial motility (Manson et al., 1977; Meister et al., 1987; Lo et al., 2007), and thus a mechanism of attraction based on inducing changes in membrane potential could apply to other bacterial species as well. To test this hypothesis, we studied the interaction of *Pseudomonas aeruginosa* cells with a pre-existing *B. subtilis* biofilm. We chose *P. aeruginosa* because it is a Gram-negative bacterium that is evolutionarily distant to Gram-positive *B. subtilis*. As expected, we find that motile *P. aeruginosa* cells also become periodically attracted to the *B. subtilis* biofilm during electrical oscillations (Figures 6A, 6B, and S6). Consistent with observations for *B. subtilis*, we find that the peak accumulation of *P. aeruginosa* motile cells at the biofilm edge again lags the peak of electrical activity in the biofilm by 22 ± 13 min (mean ± SD, n = 30 pulses) (Figure 6C). In addition, variations in the period of electrical signaling within the biofilm are directly matched by the period of *P. aeruginosa* attraction to the biofilm edge (Figure 6D). These results indicate that the mechanism of electrically

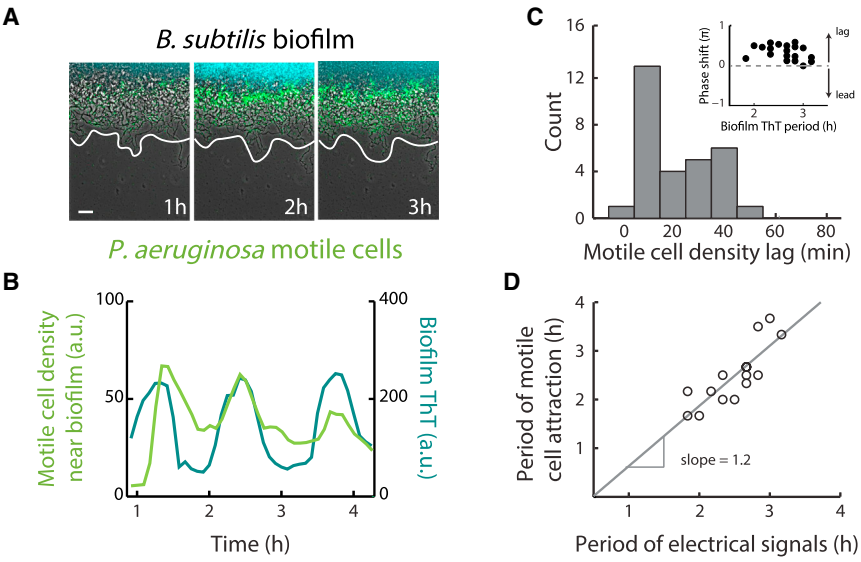

Figure 6. Biofilm Electrical Signals Can Also Attract Other Bacterial Species

(A) Film strip showing *P. aeruginosa* motile cell attraction to a pre-existing *B. subtilis* biofilm. Gray (phase contrast), cyan (membrane potential), green (*P. aeruginosa* motile cells). White line indicates the edge of the biofilm. Scale bar, 50 μm.

(B) Time series of *P. aeruginosa* motile cell accumulation (in green) near a *B. subtilis* biofilm, in phase with biofilm electrical oscillations (in cyan). Images and time series are representative of 12 independently reproduced experiments.

(C) Histogram of the time between peaks in biofilm electrical activity and peaks in *P. aeruginosa* motile cell attraction (motile cell density lag). Peaks in *P. aeruginosa* motile cell density occur on average 21.6 ± 13.4 min after the initiation of electrical oscillations within *B. subtilis* biofilms (mean ± SD, n = 30 pulses, see Quantification and Statistical Analysis in the STAR Methods). Inset: plot of the phase shift between peaks in *P. aeruginosa* attraction and *B. subtilis* electrical activity relative to the period of biofilm electrical oscillations. Arrows illustrate that a positive phase shift indicates a lag between a peak in *P. aeruginosa* attraction and biofilm electrical activity.

(D) Scatter plot of the periods of electrical oscillations within *B. subtilis* biofilms (peak to peak), and the periods of co-occurring pulses in *P. aeruginosa* motile cell attraction (peak to peak). The periods of pulses in motile cell density correlate with natural variations in the periods of electrical oscillations within biofilms (see Quantification and Statistical Analysis in the STAR Methods, Pearson correlation coefficient = 0.83, n = 16 periods).

See also Figure S6.

mediated attraction is not limited to *B. subtilis* cells and thus enables cross-species interactions.

Strength of Electrical Attraction Modulates Incorporation of New Members into a Biofilm

Attraction of distant cells to the biofilm edge could result in their incorporation into the biofilm, providing an additional opportunity to quantify the strength of electrical attraction (Figure 7A). We first confirmed that motile *B. subtilis* cells can become permanently incorporated into a pre-existing *B. subtilis* biofilm by utilizing the fluorescence labeling of motile cells (Figure 7B). We then utilized Δ*trkA* mutant biofilms that are deficient in electrical attraction to determine if reduced electrical attraction would decrease incorporation of distant cells into the biofilm. As expected, we find less permanent incorporation of *B. subtilis* cells into Δ*trkA* mutant biofilms (Figure 7C). Importantly, we find that *P. aeruginosa* cells can also become permanently incorporated into a *B. subtilis* biofilm. Consistent with *B. subtilis* motile cell results, we find less incorporation of *P. aeruginosa* motile cells into Δ*trkA B. subtilis* biofilms (Figures 7D and 7E). The strong correlation between motile cell attraction and permanent incorporation for both species confirms that incorporation accurately reflects the strength of motile cell attraction (Figures 7F and 7G). These data show that the level of permanent incorporation of new members into a pre-existing biofilm depends on the strength of electrical attraction.

DISCUSSION

Our study shows that electrical signaling mediated by potassium ion channels can extend beyond the boundaries of a biofilm to attract distant cells. This attraction is driven by dynamic gradients of potassium ions, which can alter the membrane potential of distant cells and thereby influence their motile behavior. Our work thus builds on and extends previous studies that emphasize the importance of membrane potential in bacterial motility (Miller and Koshland, 1977, 1980; Manson et al., 1977; Shioi et al., 1978, 1980; Matsuura et al., 1979; Meister et al., 1987, 1989; Lo et al., 2007). We find that long-range signaling mediated through potassium ions can generate a rapid response in cell motility, because it does not require biochemical synthesis or complex signaling networks. Given our experimental conditions, bacterial communities can effectively modulate the motility of distant cells through potassium ion channel-mediated electrical signals. These results indicate that bacterial biofilms not only regulate the behavior of cells that reside within the community, but also exert control over distant cells that are not part of the community.

Our findings show that the interaction mechanism between the biofilm and distant cells applies to even evolutionarily distant bacteria and is thus not limited to cells from a single species. In particular, the effect of extracellular potassium on membrane potential is shared among all cells, because the interaction is of physical nature. This suggests a new paradigm for long-range cross-species signaling that is generic, as it does not require specific receptors or signaling pathways. Interestingly, as a result of cross-species attraction, bacteria from a different species can become incorporated into a preexisting biofilm. Therefore, our work raises many new intriguing questions regarding the complex co-existence of biofilm communities and surrounding cells. The pursuit of these questions is likely to provide not only basic insight, but also tools that can be utilized in synthetic

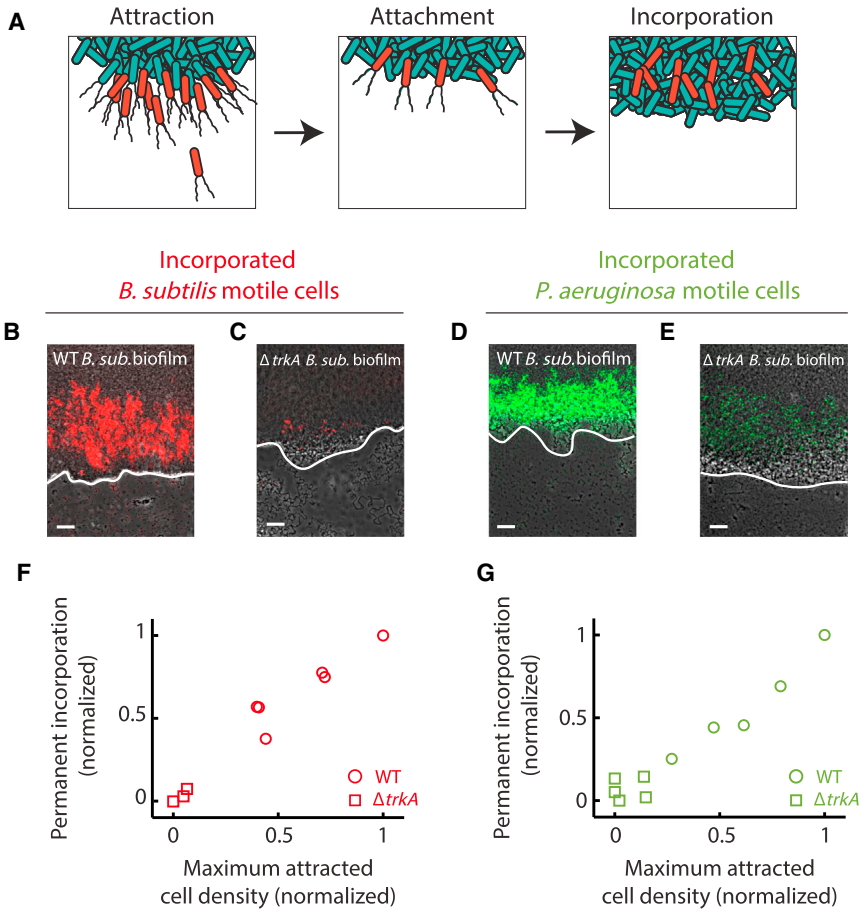

Figure 7. Attraction Can Lead to Incorporation of Motile Cells into Biofilms Depending on the Strength of the Attraction

(A) Illustration of how attraction can lead to incorporation of new cells into a pre-existing biofilm. Attracted cells (left) can remain attached to the biofilm following attraction (middle). Subsequent growth of the biofilm leads to capture of attached cells, resulting in permanent incorporation (right).

(B) Image of previously attracted *B. subtilis* motile cells (red) that have been incorporated into a pre-existing wild-type *B. subtilis* biofilm. Image is representative of six independent experiments. Incorporated cells are surrounded by cells originating from the pre-existing biofilm and are located inside the biofilm. White lines indicate biofilm edge, and biofilms are located at the top of each image. Gray (phase contrast), red (*B. subtilis* motile cells), green (*P. aeruginosa* motile cells). Scale bars, 50 μm.

(C) Image of previously attracted *B. subtilis* motile cells that have been incorporated into a pre-existing Δ*trkA* biofilm. Reduced *B. subtilis* motile cell attraction to Δ*trkA* biofilms that are deficient in electrical signaling results in diminished incorporation into the biofilm. Image is representative of six independent experiments. White lines indicate biofilm edge, and biofilms are located at the top of each image. Gray (phase contrast), red (*B. subtilis* motile cells), green (*P. aeruginosa* motile cells). Scale bars, 50 μm.

(D) Image of previously attracted *P. aeruginosa* motile cells that also became incorporated into a pre-existing *B. subtilis* biofilm. Image is representative of 12 independent experiments. White lines indicate each biofilm edge, and biofilms are located at the top of each image. Gray (phase contrast), red (*B. subtilis* motile cells), green (*P. aeruginosa* motile cells). Scale bars, 50 μm.

(E) Image of previously attracted *P.* aeruginosa motile cells that have become incorporated into a pre-existing *B. subtilis* Δ*trkA* biofilm. Diminished incorporation of *P. aeruginosa* motile cells is also observed as a consequence of reduced attraction to Δ*trkA B. subtilis* biofilms. Image is representative of five independent experiments. White lines indicate biofilm edge, and biofilms are located at the top of each image. Gray (phase contrast), red (*B. subtilis* motile cells), green (*P. aeruginosa* motile cells). Scale bars, 50 μm.

(F and G) Scatter plots comparing the average peak motile cell density during attraction to biofilms and the resulting permanent incorporation of these attracted cells into biofilms (see Quantification and Statistical Analysis in the STAR Methods). The observed direct relationship indicates that the incorporation of attracted motile cells depends on the degree of attraction. (F) Circles: *B. subtilis* motile cell attraction and incorporation into wild-type *B. subtilis* biofilms (n = 6 independently reproduced experiments). Squares: *B. subtilis* motile cell attraction and incorporation into electrical signaling deficient Δ*trkA B. subtilis* biofilms (Pearson correlation coefficient = 0.98, n = 3 independently reproduced experiments). (G) Circles: *P. aeruginosa* motile cell attraction and incorporation into wild-type *B. subtilis* biofilms (n = 6 independently reproduced experiments). Squares: *P. aeruginosa* motile cell attraction and incorporation into signaling deficient Δ*trkA B. subtilis* biofilms (Pearson correlation coefficient = 0.91, n = 5 independently reproduced experiments).

biology approaches to control the interaction of single cells and communities.

STAR★METHODS

Detailed methods are provided in the online version of this paper and include the following:

- KEY RESOURCES TABLE
- CONTACT FOR REAGENT AND RESOURCE SHARING
- EXPERIMENTAL MODEL AND SUBJECT DETAILS
  - Bacterial Strains
  - Growth conditions and dye concentrations
- METHOD DETAILS
  - Microfluidics and motile cell culturing
  - Biofilm growth
  - Motile cell growth
  - Time-lapse microscopy
  - Computational model for electrical attraction
  - Parameters of the model
- QUANTIFICATION AND STATISTICAL ANALYSIS
  - Statistical Analysis
  - Motile cell and biofilm ThT measurements
  - Motile cell density lag and oscillation period measurements
  - Permanent incorporation of attracted cells

- Membrane potential in motile cells
- Motile cell tracking

SUPPLEMENTAL INFORMATION

Supplemental Information includes six figures, one table, and four movies and can be found with this article online at http://dx.doi.org/10.1016/j.cell.2016.12.014.

An audio PaperClip is available at http://dx.doi.org/10.1016/j.cell.2016.12.014#mmc6.

AUTHOR CONTRIBUTIONS

G.M.S., J.H., and J.L. conceived of the research. J.H. and G.M.S. designed the experiments. J.H., A.P., and F.Y. performed the experiments. J.H. and J.L. performed the data analysis. L.X. and L.T. performed the mathematical modeling. J.H. and H.A.A. made the bacteria strains. G.M.S., J.H., A.P., and L.T. wrote the manuscript. All authors discussed the manuscript.

ACKNOWLEDGMENTS

We would like to thank S. Lockless, T. Cagatay, M. Asally, K. Süel, and J. Garcia-Ojalvo for comments during the writing of the manuscript, San Ly for help with strain construction, K. Pogliano and R. Losick for providing bacterial strains, and D.Y. Lee, J. Larkin, and L. Baumgart for helpful discussions. This work was in part supported by the San Diego Center for Systems Biology (NIH P50 GM085764) and the National Science Foundation (MCB-1616755). The following grants to G.M.S. funded this work: the NIH, National Institute of General Medical Sciences (R01 GM121888), the National Science Foundation (MCB-1450867 50867), the Defense Advanced Research Projects Agency (HR0011-16-2-0035), and the Howard Hughes Medical Institute-Simons Foundation Faculty Scholars program. J.H. was supported by the UCSD Cellular and Molecular Genetics Training Program through an institutional grant from the National Institute of General Medicine (T32 GM007240). A.P. was supported by a Simons Foundation Fellowship of the Helen Hay Whitney Foundation and holds a Career Award at the Scientific Interface from the Burroughs Wellcome Fund. L.X. and L.T. were partially supported by ONR grant N00014-16-1-2093.

Received: August 9, 2016
Revised: October 17, 2016
Accepted: December 9, 2016
Published: January 12, 2017

REFERENCES

Abee, T., Hellingwerf, K.J., and Konings, W.N. (1988). Effects of potassium ions on proton motive force in Rhodobacter sphaeroides. J. Bacteriol. *170*, 5647–5653.

Bakker, E.P., and Mangerich, W.E. (1981). Interconversion of components of the bacterial proton motive force by electrogenic potassium transport. J. Bacteriol. *147*, 820–826.

Berg, H.C., and Brown, D.A. (1972). Chemotaxis in Escherichia coli analysed by three-dimensional tracking. Nature *239*, 500–504.

Booth, I.R. (1985). Regulation of cytoplasmic pH in bacteria. Microbiol. Rev. *49*, 359–378.

Brameyer, S., Bode, H.B., and Heermann, R. (2015). Languages and dialects: bacterial communication beyond homoserine lactones. Trends Microbiol. *23*, 521–523.

Cao, Y., Pan, Y., Huang, H., Jin, X., Levin, E.J., Kloss, B., and Zhou, M. (2013). Gating of the TrkH ion channel by its associated RCK protein TrkA. Nature *496*, 317–322.

Castañeda-García, A., Do, T.T., and Blázquez, J. (2011). The K+ uptake regulator TrkA controls membrane potential, pH homeostasis and multidrug susceptibility in Mycobacterium smegmatis. J. Antimicrob. Chemother. *66*, 1489–1498.

Continuum Analytics (2016). Anaconda. https://www.continuum.io/.

De Jong, M.H., van der Drift, C., and Vogels, G.D. (1976). Proton-motive force and the motile behavior of Bacillus subtilis. Arch. Microbiol. *111*, 7–11.

Doyle, D.A., Morais Cabral, J., Pfuetzner, R.A., Kuo, A., Gulbis, J.M., Cohen, S.L., Chait, B.T., and MacKinnon, R. (1998). The structure of the potassium channel: molecular basis of K+ conduction and selectivity. Science *280*, 69–77.

Fell, C.J.D., and Hutchison, H.P. (1971). Diffusion coefficients for sodium and potassium chlorides in water at elevated temperatures. J. Chem. Eng. Data *16*, 427–429.

Gries, C.M., Bose, J.L., Nuxoll, A.S., Fey, P.D., and Bayles, K.W. (2013). The Ktr potassium transport system in *Staphylococcus aureus* and its role in cell physiology, antimicrobial resistance and pathogenesis. Mol. Microbiol. *89*, 760–773.

Hille, B. (2001). Ion Channels of Excitable Membranes, Third Edition (Sinauer Associates).

Hodgkin, A.L., and Huxley, A.F. (1952). A quantitative description of membrane current and its application to conduction and excitation in nerve. J. Physiol. *117*, 500–544.

Irnov, I., and Winkler, W.C. (2010). A regulatory RNA required for antitermination of biofilm and capsular polysaccharide operons in Bacillales. Mol. Microbiol. *76*, 559–575.

Jarmer, H., Berka, R., Knudsen, S., and Saxild, H.H. (2002). Transcriptome analysis documents induced competence of Bacillus subtilis during nitrogen limiting conditions. FEMS Microbiol. Lett. *206*, 197–200.

Liu, J., Prindle, A., Humphries, J., Gabalda-Sagarra, M., Asally, M., Lee, D.Y., Ly, S., Garcia-Ojalvo, J., and Süel, G.M. (2015). Metabolic co-dependence gives rise to collective oscillations within biofilms. Nature *523*, 550–554.

Lo, C.-J., Leake, M.C., Pilizota, T., and Berry, R.M. (2007). Nonequivalence of membrane voltage and ion-gradient as driving forces for the bacterial flagellar motor at low load. Biophys. J. *93*, 294–302.

Lundberg, M.E., Becker, E., and Choe, S. (2013). MstX and a putative potassium channel facilitate biofilm formation in Bacillus subtilis. PLoS ONE *8*, e60993.

Magnuson, R., Solomon, J., and Grossman, A.D. (1994). Biochemical and genetic characterization of a competence pheromone from B. subtilis. Cell *77*, 207–216.

Manson, M.D., Tedesco, P., Berg, H.C., Harold, F.M., and Van der Drift, C. (1977). A protonmotive force drives bacterial flagella. Proc. Natl. Acad. Sci. USA *74*, 3060–3064.

Mather, W., Mondragón-Palomino, O., Danino, T., Hasty, J., and Tsimring, L.S. (2010). Streaming instability in growing cell populations. Phys. Rev. Lett. *104*, 208101.

MathWorks. (2012). MATLAB and Image Processing Toolkit. https://www.mathworks.com/products/matlab/html.

Matsuura, S., Shioi, J.I., Imae, Y., and Iida, S. (1979). Characterization of the Bacillus subtilis motile system driven by an artificially created proton motive force. J. Bacteriol. *140*, 28–36.

Meister, M., Lowe, G., and Berg, H.C. (1987). The proton flux through the bacterial flagellar motor. Cell *49*, 643–650.

Meister, M., Caplan, S.R., and Berg, H.C. (1989). Dynamics of a tightly coupled mechanism for flagellar rotation. Bacterial motility, chemiosmotic coupling, protonmotive force. Biophys. J. *55*, 905–914.

Miller, M.B., and Bassler, B.L. (2001). Quorum sensing in bacteria. Annu. Rev. Microbiol. *55*, 165–199.

Miller, J.B., and Koshland, D.E., Jr. (1977). Sensory electrophysiology of bacteria: relationship of the membrane potential to motility and chemotaxis in Bacillus subtilis. Proc. Natl. Acad. Sci. USA *74*, 4752–4756.

Miller, J.B., and Koshland, D.E., Jr. (1980). Protonmotive force and bacterial sensing. J. Bacteriol. *141*, 26–32.

Paintdakhi, A., Parry, B., Campos, M., Irnov, I., Elf, J., Surovtsev, I., and Jacobs-Wagner, C. (2016). Oufti: an integrated software package for high-

accuracy, high-throughput quantitative microscopy analysis. Mol. Microbiol. *99*, 767–777.

Perego, M., Higgins, C.F., Pearce, S.R., Gallagher, M.P., and Hoch, J.A. (1991). The oligopeptide transport system of Bacillus subtilis plays a role in the initiation of sporulation. Mol. Microbiol. *5*, 173–185.

Plásek, J., and Sigler, K. (1996). Slow fluorescent indicators of membrane potential: a survey of different approaches to probe response analysis. J. Photochem. Photobiol. B *33*, 101–124.

Preibisch, S., Saalfeld, S., and Tomancak, P. (2009). Globally optimal stitching of tiled 3D microscopic image acquisitions. Bioinformatics *25*, 1463–1465.

Prindle, A., Liu, J., Asally, M., Ly, S., Garcia-Ojalvo, J., and Süel, G.M. (2015). Ion channels enable electrical communication in bacterial communities. Nature *527*, 59–63.

Roosild, T.P., Miller, S., Booth, I.R., and Choe, S. (2002). A mechanism of regulating transmembrane potassium flux through a ligand-mediated conformational switch. Cell *109*, 781–791.

Schindelin, J., Arganda-Carreras, I., Frise, E., Kaynig, V., Longair, M., Pietzsch, T., Preibisch, S., Rueden, C., Saalfeld, S., and Schmid, B. (2012). Fiji: an open-source platform for biological-image analysis. Nat. Methods *9*, 676–682.

Schlösser, A., Hamann, A., Bossemeyer, D., Schneider, E., and Bakker, E.P. (1993). NAD+ binding to the Escherichia coli K(+)-uptake protein TrkA and sequence similarity between TrkA and domains of a family of dehydrogenases suggest a role for NAD+ in bacterial transport. Mol. Microbiol. *9*, 533–543.

Shapiro, J.A. (1998). Thinking about bacterial populations as multicellular organisms. Annu. Rev. Microbiol. *52*, 81–104.

Shioi, J.I., Imae, Y., and Oosawa, F. (1978). Protonmotive force and motility of Bacillus subtilis. J. Bacteriol. *133*, 1083–1088.

Shioi, J.I., Matsuura, S., and Imae, Y. (1980). Quantitative measurements of proton motive force and motility in Bacillus subtilis. J. Bacteriol. *144*, 891–897.

Trackpy Authors (2016). Trackpy. http://soft-matter.github.io/trackpy/v0.3.2/#.

Volfson, D., Cookson, S., Hasty, J., and Tsimring, L.S. (2008). Biomechanical ordering of dense cell populations. Proc. Natl. Acad. Sci. USA *105*, 15346–15351.

Waters, C.M., and Bassler, B.L. (2005). Quorum sensing: cell-to-cell communication in bacteria. Annu. Rev. Cell Dev. Biol. *21*, 319–346.

Yasbin, R.E., and Young, F.E. (1974). Transduction in Bacillus subtilis by bacteriophage SPP1. J. Virol. *14*, 1343–1348.

Yi, T.-M., Huang, Y., Simon, M.I., and Doyle, J. (2000). Robust perfect adaptation in bacterial chemotaxis through integral feedback control. Proc. Natl. Acad. Sci. USA *97*, 4649–4653.

STAR★METHODS

KEY RESOURCES TABLE

REAGENT or RESOURCE	SOURCE	IDENTIFIER
Chemicals, Peptides, and Recombinant Proteins		
Potassium chloride	Sigma-Aldrich	Cat #: P3911, CAS: 7447-40-7
L-glutamic acid monosodium salt hydrate	Sigma-Aldrich	Cat #: G5889, CAS: 142-47-2 (anhydrous)
Glycerol	Sigma-Aldrich	Cat #: G5516, CAS: 56-81-5
Magnesium chloride hexahydrate	Fisher Scientific	Cat #: BP214, CAS: 7786-30-3
Potassium phosphate monobasic	Fisher Scientific	Cat #: BP362, CAS: 7778-77-0
Potassium phosphate dibasic	Fisher Scientific	Cat #: BP363, CAS: 7758-11-4
Thiamine HCl	Fisher Scientific	Cat #: BP892, CAS: 67-03-8
Manganese chloride	Acros Organics	Cat #: AC193451000, CAS: 13446-34-9
Calcium chloride	Fisher Scientific	Cat #: BP510, CAS: 10035-04-8
Iron (III) chloride	Acros Organics	Cat #: AC217090025, CAS10025-77-1
Zinc (II) chloride	Sigma-Aldrich	Cat #: Z0152, CAS: 7646-85-7
Thioflavin T	Acros Organics	Cat #: AC211761000, CAS: 2390-54-7
Isopropyl β-D-1-thiogalactopyranoside	Sigma-Aldrich	Cat #: IPTG-RO, CAS: 367-93-1
Asante Potassium Green (AM)	TEFLabs	Cat #: 3602
MOPS	Sigma-Aldrich	Cat #: M3183, CAS: 1132-61-2
Experimental Models: Organisms/Strains		
B. subtilis NCIB 3610	Bacillus Genetic Stock Center	BGSCID: 3A1
B. subtilis NCIB 3610 *AmyE::*P_{hyp}*-mKate2, sinI::neo* (motile cells)	This study	N/A
B. subtilis NCIB 3610 *AmyE::*P_{hyp}*-YFP, hag::cat* (non-motile cells)	This study	N/A
B. subtilis NCIB 3610 *trkA::neo* (*ΔtrkA*)	Prindle et al., 2015	N/A
B. subtilis NCIB 3610 *AmyE::*P_{hyp}*-mKate2, ktrA::mls (ΔktrA)*	This study	N/A
P. aeruginosa PA01/pJA06-miniRK2 P_{Spac}*-tdTomato::kan*	This study	N/A
Software and Algorithms		
MATLAB and Image Processing Toolkit	MathWorks, 2012	https://www.mathworks.com/products/matlab/html
Python (Anaconda)	Continuum Analytics, 2016	
Trackpy	Trackpy Authors, 2016	http://soft-matter.github.io/trackpy/v0.3.2/#
FIJI and Stitching Plugin	Schindelin et al., 2012; Preibisch et al., 2009	https://fiji.sc/
Oufti	Paintdakhi et al., 2016	http://oufti.org/
Other		
CellASIC Y04D microfluidic plates	EMD Millipore	Cat #: Y04D-02-5PK
CellASIC ONIX microfluidic platform	EMD Millipore	Cat #: EV262

CONTACT FOR REAGENT AND RESOURCE SHARING

Requests for strains and further information can be directed to the Lead Contact, Gürol M. Süel (gsuel@ucsd.edu).

EXPERIMENTAL MODEL AND SUBJECT DETAILS

Bacterial Strains

All experiments were performed using the *Bacillus subtilis* strain NCIB 3610 and the *Pseudomonas aeruginosa* strain PA01. *B. subtilis* 3610 was a kind gift from W. Winkler (University of Maryland) (Irnov and Winkler, 2010). *P. aeruginosa* PA01 was a kind gift from K. Pogliano (University of California, San Diego) and contained a td-Tomato fluorescent reporter plasmid which was made by J. Aguilar (University of California, San Diego). All strains used in this study can be found in Table S1 and were derived from *B. subtilis* 3610 or *P. aeruginosa* PA01. *B. subtilis* motile cells contained an mKate2 reporter under the control of the inducible P_{hyp} promoter (1 mM IPTG was used for induction). In addition, the *sinI* gene (regulator of biofilm formation) was deleted in motile cells in order to reduce clogging in the device. The mKate2 construct was a kind gift from R. Losick. The *ΔtrkA* and *Δhag* strains were made by PCR amplifying 1 kb regions upstream and downstream of the gene to be deleted and cloning them into the pER449 vector (gift from W. Winkler) flanking an antibiotic resistance cassette. Constructs were sequence verified and chromosomally integrated using a standard one-step transformation procedure (Jarmer et al., 2002). The *ΔktrA* strain was made by obtaining the KtrA deletion strain BKE31090 from the Bacillus Genetic Stock Center and using it as a donor to move the *ΔktrA::mls* construct into strain 3610 via SPP1-mediated phage transduction into the 3610 background (Yasbin and Young, 1974). For *ΔktrA* and *Δhag* cells, a constitutive reporter was then chromosomally integrated using the one-step transformation procedure. Integrations were confirmed by colony PCR.

Growth conditions and dye concentrations

Biofilms were grown in MSgg medium: 5 mM potassium phosphate buffer (pH 7.0), 100 mM MOPS buffer (pH 7.0, adjusted with NaOH), 2 mM $MgCl_2$, 700 μM $CaCl_2$, 50 μM $MnCl_2$, 100 μM $FeCl_3$, 1 μM $ZnCl_2$, 2 μM thiamine HCl, 0.5% (v/v) glycerol, and 0.5% (w/v) monosodium glutamate. MSgg medium was made fresh from stocks the day of the experiment. Glutamate and iron stocks were made fresh weekly. ThT (Sigma-Aldrich) was used at a final concentration of 10 μM and APG-4 (TEFLabs) was used at 2 μM. The P_{hyp} reporter used in motile cells was induced using 1 mM IPTG. Biofilms were acclimated for at least 1 hr to any dyes and inducers used in the experiment before addition of motile cells.

METHOD DETAILS

Microfluidics and motile cell culturing

B. subtilis biofilms were grown to a mature state (~20h of growth), and then a separately grown planktonic cell culture of either *B. subtilis* or *P. aeruginosa* was introduced into the growth chamber with the biofilm.

Biofilm growth

For microfluidic culturing, we used a CellASIC ONIX Microfluidic Platform and Y04D microfluidic plates (EMD Millipore). The day before growing biofilms, the strain to be used was streaked out onto LB agar plates from −80°C glycerol stocks. The following day, a single colony was picked from the biofilm strain plate and inoculated in 3 mL lysogeny broth (LB). After 3h of growth shaking at 37°C, cells were spun down at 2100 rcf for 1 min, re-suspended in fresh MSgg and loaded into the microfluidic chamber. After loading, cells were incubated at 32.5°C overnight, then 30°C for the rest of the experiment. Prior to addition of motile cells, biofilms were grown with media supplied at 1.5 psi from one well.

Motile cell growth

Motile cell strains to be used were streaked out onto LB agar plates from −80°C glycerol stocks. The same night as biofilms were initially loaded and growing, a single colony of the *B. subtilis* motile cell strain to be used was inoculated in 3 mL of MSgg + 1 mM IPTG and any fluorescent reporters such as ThT or APG-4 to be used in the experiment. This culture was grown overnight (10-14 h) in a 15 mL culture tube shaking at 37°C. In the morning, the culture was re-suspended in fresh MSgg and immediately loaded into the microfluidic chamber. Non-motile *Δhag B. subtilis* cells were cultured and introduced into the microfluidic device in the same manner as motile *B. subtilis* cells. *P. aeruginosa* motile cells were cultured in the same way as *B. subtilis,* except after growth overnight, the culture was diluted 1:30 in fresh MSgg and allowed to grow at 37°C shaking for 2 hr before re-suspending in fresh MSgg, and loading into the microfluidic chamber.

After the onset of oscillations in the mature biofilm, motile cells were introduced into the microfluidic chamber. The OD of motile cells was measured and normalized to 1 for *B. subtilis* and 0.5 for *P. aeruginosa*. Motile cells were passed through a 5 μm filter to remove any cell aggregates, spun down at 2100 rcf for 1 min, and resuspended in fresh MSgg + 1 mM IPTG + fluorescent dyes. Motile cells were allowed to flow into the chamber through a dedicated media inlet well. The flow rate (12 μm/sec) was low enough to supply the growth chamber with fresh media while not being so fast that it prevented motile cells from being able to swim upstream against the flow.

The potassium addition experiment shown in Figure 2 was performed by growing a single biofilm on one side of the growth chamber and introducing an artificial potassium source into the other side of the chamber. In addition to the inlet used to flow in the motile cell suspension, a potassium concentration gradient could be produced by flowing MSgg supplemented with 300 mM KCl from the inlet furthest from the biofilm.

Time-lapse microscopy

Growth of biofilms was tracked using phase contrast microscopy and motile cell behavior was tracked by fluorescence microscopy of the *P_{hyp}-mKate2* reporter (only present in motile cells). The imaging systems used were Olympus IX83 with an X-Cite LED light source from Lumen Dynamics and Olympus IX81 with a Lambda XL light source from Sutter Instruments. Attraction experiments were acquired using a 10X objective and a 40X objective was used to evaluate ThT intensity in motile cells for the experiments shown in Figures 4C, 4D, and 5D. During time lapse experiments, phase and fluorescence images were taken in 10 min intervals.

Computational model for electrical attraction

Our agent-based model assumes that each motile cell changes its electrophysiological state and motility independently of each other and only in response to changes in extracellular potassium. We describe intracellular potassium-driven dynamics within each cell using a generalization of the electrophysiological model introduced in our earlier paper (Prindle et al., 2015). The membrane potential is governed by the standard Hodgkin-Huxley-type conductance equation

$$\eta C\frac{dV}{dt} = -g_K n^4(V-V_K) - g_L(V-V_L) \tag{1}$$

in which C is the capacitance of the cell membrane. The first term in the right hand side describes the change in membrane potential by potassium ions escaping the cell through potassium ion channels, while the second term describes the leak current. In the standard Hodgkin-Huxley model, the membrane potential dynamics are very fast (milliseconds), much faster than the slow changes in extracellular potassium and corresponding changes in bacterial motility (hours). Since it is very difficult to simulate together processes of such vastly different timescales, we introduced a scaling factor η to slow down the intracellular electrophysiological dynamics. The scaling factor is also applied to Equations 3 and 4. As long as the electrophysiological processes remain much faster than the slow part of the model, this did not have an appreciable effect on the slow dynamics of the cellular population. We used the value η=300 and verified that changing this factor to 150 did not appreciably affect the results of our simulations.

The resting potentials V_k and V_L are set by the ion pumps, and generally are dependent on both intra- and extracellular potassium levels, for which we assume a simple linear form,

$$V_K = V_{K0} + \delta_K(K_e + K_i);\quad V_L = V_{L0} + \delta_L(K_e + K_i). \tag{2}$$

The fourth power in the first term of (1) stems from the fact (Doyle et al., 1998) that bacterial potassium channels are formed by four subunits, which on average are open during a fraction of time n whose dynamics is given by the following rate equation:

$$\frac{\eta dn}{dt} = \alpha(S)(1-n) - \beta n \tag{3}$$

where the first term describes channel opening and the second term specifies the rate of channel closing. As in Prindle et al. (2015), the opening rate α of the potassium channel is assumed to depend on metabolic stress, S, according to the Hill function $\alpha(S) = \alpha_0 S^m/(S_{th}^m + S^m)$. This metabolic stress variable that stands for the concentration of stress-related metabolic products (Cao et al., 2013), such as excess NAD^+ (Roosild et al., 2002; Schlösser et al., 1993) is itself controlled by the membrane potential according to the equation

$$\frac{\eta dS}{dt} = \frac{\alpha_s(V_{th}-V)}{\exp\left(\frac{V_{th}-V}{\sigma}\right)-1} - \gamma_s S. \tag{4}$$

In departure from our previous model (Prindle et al., 2015) that described time-dependent dynamics of the extracellular potassium in the dense biofilm environment, here we assume that motile cells have sufficiently low density and therefore do not change the extracellular potassium appreciably. Instead, we focus on the concentration of the intracellular potassium K_i,

$$\frac{dK_i}{dt} = -\varepsilon g_K n^4(V-V_K) + \beta_K(V_0 - V) \tag{5}$$

where the first term describes the flux of potassium through ion channels and the second term describes the action of potassium pumps which maintain the membrane potential at the resting value V_0. The second term only appears when $V_0 > V$ and is zero otherwise, because the ion pump can only pump the potassium from outside to inside of a cell.

It can be shown that the regulation of the intracellular potassium described by Equation 5 plays the role of the integral feedback control loop similar to other mechanisms of bacterial chemotaxis (Yi et al., 2000). Indeed, in the absence of stress ($S \approx 0$), the ion channels are closed ($n \approx 0$), and the membrane potential equilibrates near $V = V_0$ independently of the level of extracellular potassium (perfect adaptation). However, a change in extracellular potassium levels may cause complex transient changes in the membrane potential. When extracellular potassium level rises, according to Equation 1 it slightly depolarizes the cell (increases V). The

depolarization causes opening of the ion channels $(n > 0)$, intracellular potassium flushes out according to Equation 5, and the cell becomes strongly hyperpolarized. Then the channels close, and the ion pumps restore the membrane potential to the resting value. If the level of extracellular potassium continues to rise, the process repeats, and a periodic sequence of depolarization pulses ensues (see Figure S5). If the level of extracellular potassium slowly decreases, it slightly hyperpolarizes the cell, but the channels remain closed, and the ion pump maintains the membrane potential close to the resting value. These transient changes in the membrane potential lead to changes in intracellular energy levels (we can think of this energy as PMF or ATP) and in turn lead to changes in the bacterial motility. We describe the energy dynamics by the simple relaxation equation

$$\frac{dE}{dt} = -\alpha_E V - \gamma_E E \tag{6}$$

and postulate that the tumbling probability is downregulated by the energy:

$$\mathcal{P} = \frac{K_E^q}{(E - E_0)^q + K_E^q}. \tag{7}$$

The strong anisotropy in the dynamics of the membrane potential for increasing and decreasing extracellular potassium leads to the chemotactic response of motile bacteria to the spatial gradient of potassium. Indeed, if a cell swims up the gradient, it experiences rising levels of potassium and strongly hyperpolarizes, thus increasing the mean proton motive force and the level of energy in the cell. Therefore, its tumbling probability diminishes, and the cell continues to swim in the same direction. However, when the cell swims down the potassium gradient, hyperpolarization does not occur, and the tumbling probability remains high.

To simulate bacterial motion, we adapted the mechanical agent-based model developed in our earlier work (Volfson et al., 2008; Mather et al., 2010). Each cell is modeled as a spherocylinder of unit diameter that grows linearly along its axis and divides equally after reaching a critical length $l_d = 4$. It can also move along the plane due to forces and torques produced by interactions with other cells and its own flagellae-mediated motility (however, we do not model the flagella dynamics explicitly). The slightly inelastic cell-cell normal contact forces are computed via the standard spring-dashpot model, and the tangential forces are computed as velocity-dependent friction. During periods of directed motion, the cell experiences a self-propelling force directed along its axis. During the periods of tumbling, the self-propelling directional force is switched off, and the cell experiences a strong random torque which quickly turns it in a random new direction. The probability of switching from directed motion to tumbling for each cell is controlled by variable $\mathcal{P}$ that is computed from the electrophysiological cell model. Biofilm-bound cells were assumed to be non-motile (no self-propelling force, no tumbling torque).

The dynamics of extracellular potassium ion field were implemented via a reaction-diffusion model where the biofilm cells played the role of sources and sinks of potassium periodically,

$$\frac{\partial K_e(\boldsymbol{r})}{\partial t} = \sum_j f(t)\delta(\boldsymbol{r} - \boldsymbol{r}_j) + D_k \nabla^2 K_e(\boldsymbol{r}). \tag{8}$$

Here K_e is the extracellular potassium concentration and $\boldsymbol{r}_j$ is the location of the j-th cell, $f(t)$ is the periodic function describing periodic excretion (with rate α_k) and absorption (with rate $-\beta_k K_e$) cycles of extracellular potassium by the biofilm cells, and D_k is the potassium diffusion constant (Fell and Hutchison, 1971).

Each simulated motile "cell" carried a set of Equations 1, 2, 3, 4, 5, 6, and 7 describing its membrane potential dynamics in response to the local extracellular potassium concentration. The effect of the motile cells on the extracellular potassium concentration was ignored. The parameters of the model are shown in Table S1.

We performed multiple simulations in a narrow channel of length 100 and width 20 (Figure 5B). The biofilm consisting of approximately 200 cells was initially grown in the back of the open channel (100 × 20 μm^2), after which 100 motile cells were introduced into the open space of the channel. Of course, this computational domain represents only a small portion of the microfluidic chamber used in experimental studies, so our computational results only can be interpreted on a semiquantitative level, as a way to reveal and explore the underlying biophysical mechanism of the potassium-driven chemotaxis. For simplicity, we also neglected growth and division for motile cells and only considered their motion in response to the external potassium changes. We used periodic boundary conditions on the side walls for motile cells: when a motile cell touches the left wall, it disappears and reappears at the right side and vice versa. The non-motile biofilm cells were periodically switched between producing and absorbing potassium.

A typical simulation is shown in Movie S4. At each time step we computed the average concentration of potassium and the motile cell density near the biofilm edge. The periodic oscillations of cell density are clearly seen, which indicate the chemotactic response of bacteria to the potassium oscillations. The distribution of the proton motive force shifts between the peak and the trough phases (Figure 5C), in agreement with experimental findings (Figure 5D).

Parameters of the model

The aim of the computational model is to reproduce the observed phenomenology semiquantitatively. Since the electrophysiology of bacterial cells is much less studied than of their mammalian counterparts, the parameters of the electrophysiological equations were

taken either from the classical literature (Hodgkin and Huxley, 1952) or our earlier model describing potassium signaling in bacteria (Prindle et al., 2015). Some parameters (such as resting membrane potentials) were deduced from direct measurements. Other model parameters that connect electrophysiology and motility (marked as "fitting") were chosen by random parameter search within physiologically relevant ranges and then further improved by manual variation to maximize the agreement with experimental observations.

QUANTIFICATION AND STATISTICAL ANALYSIS

FIJI/ImageJ (Schindelin et al., 2012; Preibisch et al., 2009) and MATLAB (MathWorks, 2012) were used for image analysis. Biofilm growth, motile cell density at the biofilm edge, and ThT/APG-4 intensity were obtained using the MATLAB image analysis toolbox.

Statistical Analysis

Statistical analysis was performed using MATLAB. p values of < 0.05 were considered to be statistically significant. To determine whether data met assumptions of the statistical tests used, MATLAB's skewness and kurtosis functions were used. Datasets did not have excessive skew or kurtosis and thus were assumed to be normally distributed.

Motile cell and biofilm ThT measurements

Phase contrast images were used to determine the coordinates of the biofilm edge. Based on the coordinates of the biofilm edge, a 100 μm wide region was established both inward (toward biofilm interior) and outward from the biofilm edge (See illustration in Figure 1A). The 100 μm region inside the biofilm was used to measure ThT intensity within the biofilm and the 100 μm region outside the biofilm was used to measure motile cell fluorescent reporter intensity in the region immediately surrounding the biofilm. The average intensities obtained from these regions were reported as the biofilm ThT and motile cell density near biofilm time traces. The motile cell density values were normalized to the density of the cell suspension introduced into the device. ThT traces were detrended using MATLAB's "detrend" function. Specifically, the function fits a least-squares line to the data and subtracts this linear trend from the data.

The motile cell response reported in Figure 3D was obtained by averaging the intensities of motile cell attraction peaks from multiple experiments to obtain a single motile cell response measurement. The biofilm signal average reported in Figure 3D was obtained in a similar way, by averaging the intensities of ThT peaks for multiple experiments into a single maximum biofilm ThT measurement. A similar analysis was done for Figures 7F and 7G, except the peak intensities of attracted motile cells were averaged for each independent biofilm so that they could be compared to the resulting permanent incorporation of attracted cells for that biofilm. For all these measurements, the exact value of n is presented in the corresponding figure legend and represents the number of independent experiments of each genetic background used.

Motile cell density lag and oscillation period measurements

The motile cell density lag measurements reported in Figures 1D and 6C were obtained using the peak of motile cell attraction and biofilm ThT. Lag was defined as the time between a biofilm ThT peak and the corresponding peak in motile cell attraction. Positive lag times indicate that a peak in motile cell attraction occurred after a peak in biofilm ThT. For Figures 1D and 6C the exact value of n is presented in the corresponding figure legends and represents the number of peaks of ThT and corresponding attraction shown in the histogram. The period comparisons reported in Figures 1E and 6D were obtained by determining the period, peak-to-peak, of oscillations in biofilm ThT and motile cell attraction. The period of motile cell attraction was then plotted versus the period of the corresponding pulse in biofilm ThT. For Figures 1E and 6D, the exact value of n is presented in the corresponding figure legends and represents the number of periods, peak-to-peak, of oscillations and corresponding attraction included in the plot.

Permanent incorporation of attracted cells

The permanent incorporation of attracted cells reported in Figures 7F and 7G was obtained by measuring the average fluorescence intensity of mKate2 (a reporter only present in motile cells) in the 100 μm region immediately inward from the biofilm edge (toward biofilm interior) and normalizing by the area of the evaluated region and the density of the motile cell suspension flowing into the device. Incorporation measurements were obtained at the conclusion of each experiment. The exact value of n is presented in the corresponding figure legend and represents the number of independent experiments included in each plot.

Membrane potential in motile cells

Data for Figure 5D was obtained by segmenting motile cells and obtaining ThT fluorescence intensity for each cell using the Oufti software (Paintdakhi et al., 2016) and MATLAB.

Motile cell tracking

Single cell trajectories for the evaluation of tumbling frequency in motile cells were obtained by analyzing time lapse phase contrast image stacks taken at 10 ms intervals at 40X magnification. The Python based cell tracking software TrackPy and the Anaconda

Python platform (Trackpy Authors, 2016; Continuum Analytics, 2016) were used to track single cell movement over time and compile this movement into trajectories for each tracked cell. We included trajectories for cells that were tracked for 500 ms or longer in Figures 4E and 4F. The exact value of n is presented in the corresponding figure legend and represents the number of motile cell trajectories obtained during the peak and trough of electrical activity. Trajectories obtained with TrackPy were further analyzed using MATLAB. Tumbling events were determined by finding the angle of rotation between each time point of the trajectory and if this rotational angle was greater than 60 degrees, it was called a tumbling event. Tumbling frequencies are reported as number of tumbling events per second.

Cell

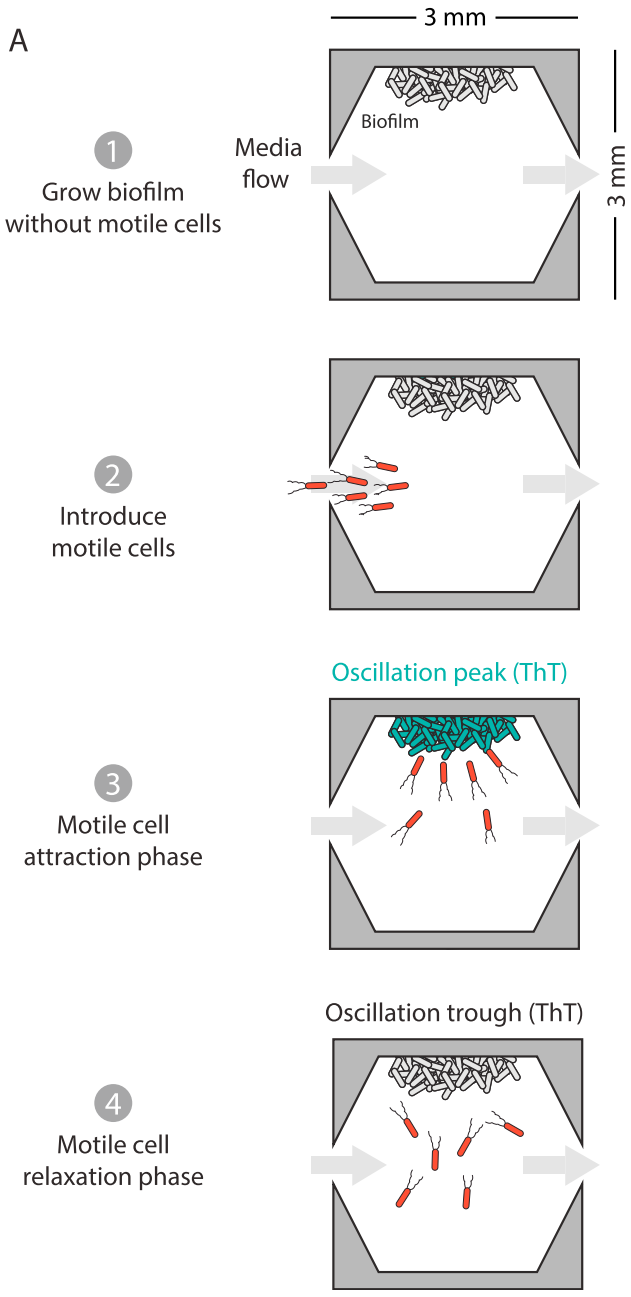

Figure S1. Related to Figure 1

Outline of the experimental procedure used to measure the interaction dynamics between biofilms and motile cells. The microfluidic device used in our experiments has a growth chamber that measures 3mm x 3mm x 6 μm (X x Y x Z). Biofilms grow from a side wall outward as illustrated, and media flows through the device at a rate of 12 μm/s. Step 1, grow biofilm without motile cells until it reaches critical size for oscillations. Step 2, introduce motile cells into growth chamber with the biofilm. Step 3-4, as oscillations occur, we image biofilm electrical oscillations with the fluorescent membrane potential reporter Thioflavin T (ThT) and motile cell movement with a fluorescent constitutive reporter *Phyp-mKate2*. Depending on the phase of oscillations (peak or trough), we see periodic attraction of motile cells toward the biofilm.

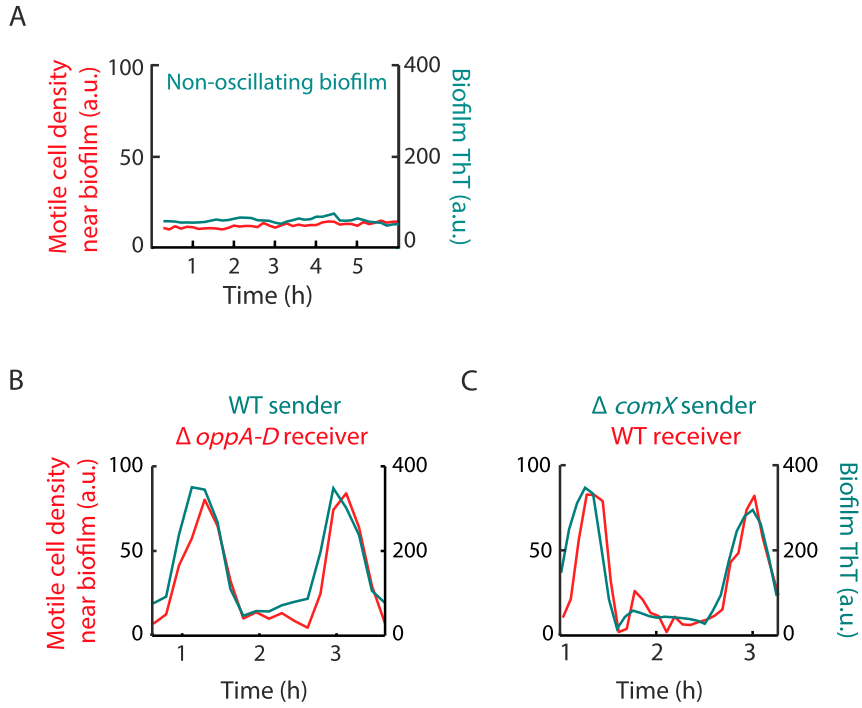

Figure S2. Related to Figure 1

(a) Time series of motile cell density near a biofilm that has not yet initiated electrical oscillations, and corresponding membrane potential in the biofilm. Motile cells fail to respond to a biofilm that has not yet initiated electrical oscillations. Time series is representative of 3 independently reproduced experiments. (b) Time series of *ΔoppA-D* motile cells (receivers) responding to a wild-type biofilm (sender). The *oppA-D* operon encodes the transporter required for the uptake of the major quorum-sensing peptide family (*phr*) (Perego et al., 1991), and we observed no effect of this deletion on motile cell attraction. (c) Time series of wild-type motile cells responding to a *ΔcomX* biofilm also shows no effect on motile cell attraction. The *comX* gene encodes one of the best characterized quorum-sensing signaling peptides (Magnuson et al., 1994), and we again observed no effect of this deletion on motile cell attraction.

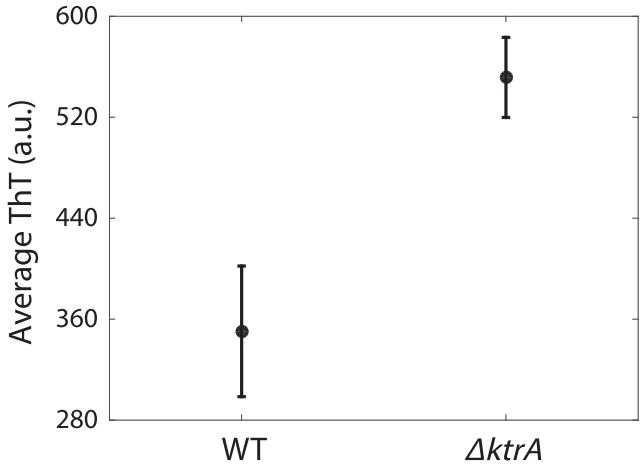

Figure S3. Related to Figure 3

Deletion of the KtrA potassium pump in *B. subtilis* results in hyperpolarization of membrane potential. Plot of average ThT in wild-type (WT) and *ΔktrA* cells (n = 2 *ΔktrA* biofilms, 1 WT biofilm ± st. dev.).

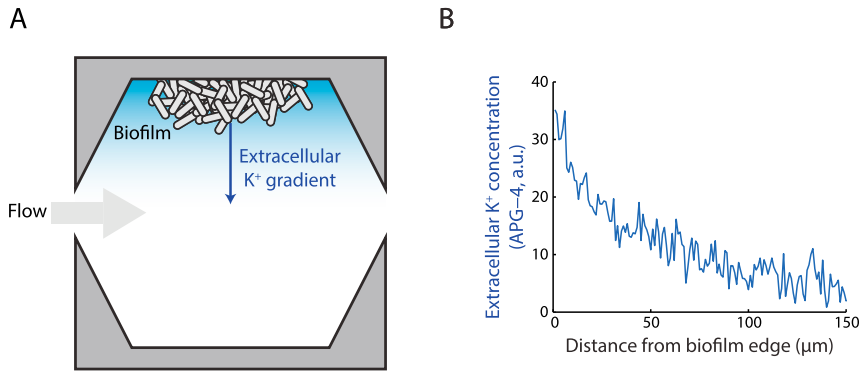

Figure S4. Related to Figure 4

(a) Illustration of the extracellular potassium gradient (blue shading) formed by biofilms in the microfluidic device. The blue arrow illustrates the biofilm region measured experimentally in (b), and the gray arrow indicates the flow of media relative to biofilm growth and potassium diffusion. (b) Plot of extracellular potassium produced by the biofilm as a function of distance from the biofilm edge shows a gradient in extracellular potassium. Extracellular potassium is measured with the extracellular potassium specific dye APG-4.

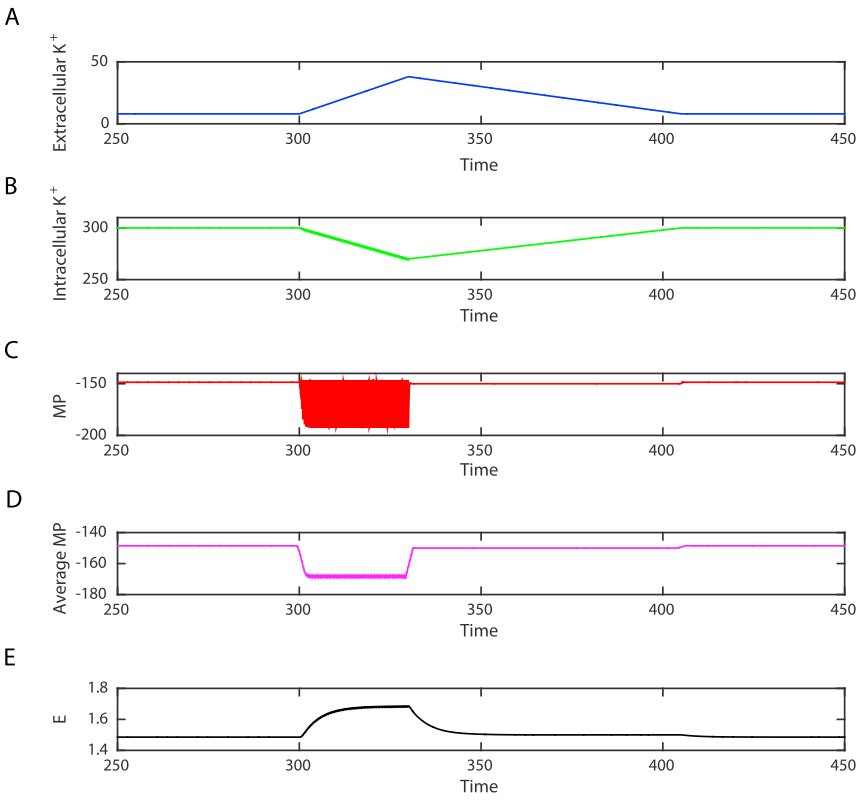

Figure S5. Related to Figure 5

(a-e) Mathematical modeling of the motile cell response to extracellular potassium released by a biofilm. (a) Extracellular potassium emitted from the biofilm over time. (b) Intracellular potassium in motile cells over time. (c) Instantaneous membrane potential (MP) in motile cells over time. (d) Average membrane potential in motile cells over time. (e) Average energy in motile cells over time.

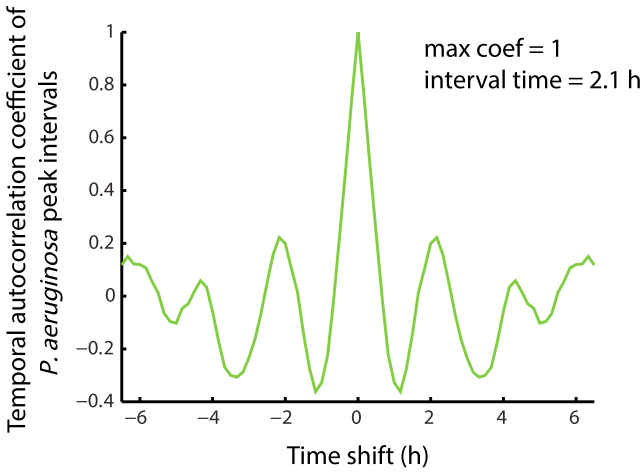

Figure S6. Related to Figure 6

Representative temporal autocorrelation coefficient of oscillations in *P. aeruginosa* motile cell attraction shows periodicity and an average peak interval time of 2.1 hr.